Multishock to Quasi-Isentropic Compression of Dense Gaseous Deuterium-Helium Mixtures up to 120 GPa: Probing the Sound Velocities Relevant to Planetary Interiors

Guo-Jun Li,[1,2] Zhi-Guo Li,[1,*] Qi-Feng Chen,[1,†] Yun-Jun Gu,[1] Wei Zhang,[3] Lei Liu,[3,‡] Hua-Yun Geng,[1] Zhao-Qi Wang,[1,2] Yang-Shun Lan,[1,2] Yong Hou,[4] Jia-Yu Dai,[4] and Xiang-Rong Chen[2]

[1]*National Key Laboratory for Shock Wave and Detonation Physics, Institute of Fluid Physics, Chinese Academy of Engineering Physics, Mianyang 621900, China*

[2]*College of Physics, Sichuan University, Chengdu 610065, China*

[3]*School of Science, Southwest University of Science and Technology, Mianyang 621010, China*

[4]*Department of Physics, National University of Defense Technology, Changsha 410073, China*

(Received 30 July 2020; revised 16 November 2020; accepted 8 January 2021; published 15 February 2021)

Shock reverberation compression experiments on dense gaseous deuterium-helium mixtures are carried out to provide thermodynamic parameters relevant to the conditions in planetary interiors. The multishock pressures are determined up to 120 GPa and reshock temperatures to 7400 K. Furthermore, the unique compression path from shock-adiabatic to quasi-isentropic compressions enables a direct estimation of the high-pressure sound velocities in the unexplored range of 50–120 GPa. The equation of state and sound velocity provide particular dual perspectives to validate the theoretical models. Our experimental data are found to agree with several equation of state models widely used in astrophysics within the probed pressure range. The current data improve the experimental constraints on sound velocities in the Jovian insulating-to-metallic transition layer.

DOI: 10.1103/PhysRevLett.126.075701

The study of gas giant planets such as Jupiter and Saturn in our Solar System is an essential topic in astrophysics. Hydrogen and helium are the major constituents of these planets. Accurate knowledge of key thermodynamic properties of hydrogen, helium, and their mixtures at extremely high pressures and temperatures, such as their equations of state (EOSs) and the velocities of sound in these media, is crucial for the understanding of gas giants [1–6]. Enormous efforts have been made toward building the EOSs of H_2-He mixtures for astrophysical applications. So far, widely used models include the semianalytical model by Saumon, Chabrier, and van Horn (SCVH) [7], the *ab initio* EOS of Militzer and Hubbard [8], and the global multiphase EOS of the Rostock group (REOS.3) [9]. Recently, a new EOS was proposed by Chabrier, Mazevet, and Soubiran (CMS) [10] in which entropy was calculated over a wide density-temperature domain. Miguel *et al.* [11] and Debras *et al.* [12] explored the internal structure of Jupiter using these EOSs and found that significant differences existed between them and the derived interior models of Jupiter, showing that there is a strong need to constrain the H_2-He EOS at the extreme pressures relevant to planetary interiors.

Shock compression experiments are paramount in providing accurate experimental constraints to verify and validate these theoretical models. Various experimental loading techniques, including a two-stage light-gas gun [13–17], convergent explosives [18–21], a magnetically launched flyer [22–24], and laser-driven shocks [25–31], have been directed toward helium, hydrogen, and deuterium, and the EOSs have been determined up to TPa pressures. Nevertheless, these experiments have mainly focused on pure hydrogen, deuterium, and helium, which is very far from being enough to constrain the properties of their mixtures because of the complicated interactions between their components [32,33]. Li *et al.* [34,35] and Gu *et al.* [36] performed shock experiments on H_2-He and D_2-He mixtures to validate the EOS models widely used in astrophysics, but these experimental EOS data are limited to pressures below 60 GPa. Besides, the measurement of the sound velocities in hydrogen (deuterium), helium, and their mixtures at elevated pressure-temperature conditions that are capable of providing significant information about phase transitions and direct constraints on the seismic structure of giant planets [37], is more complicated and challenging. Until now, very few experimental measurements of the sound velocities in pure hydrogen, helium, and deuterium have been made [37–41], and none have been obtained for their mixtures. Overall, the shock compression experiments that have been conducted on H_2-He or D_2-He mixtures are severely insufficient, and the available data were obtained far below the pressures and temperatures that exist in the interiors of the majority of gas giants. For this Letter, we designed and performed shock-reverberation compression experiments on dense D_2-He mixtures. A simultaneous measurement of the EOS and sound velocity was achieved for pressures exceeding 100 GPa. These EOS and sound velocity data provide important benchmarks

for the current popular theoretical models and would be beneficial to understanding the material properties relevant to planetary interiors.

Reverberating shock experiments were performed using a two-stage light-gas gun. The D_2-He gases with mole ratios of 1 : 1 and 3 : 1 are precompressed up to 40 MPa and sealed in a sandwich-structured target assembly. Strong planar shock waves are generated through the impact of a high-velocity tantalum (Ta) flyer into the baseplate of the target. The shock wave transmits into the D_2-He sample across the baseplate and then reverberates repeatedly between the baseplate and the window due to these materials having higher shock impedances than the D_2-He sample. The light radiance emitted from the multishocked sample is delivered to two sets of multichannel optical pyrometers (MCOP) [42]. Two sets of velocity interferometry devices (Doppler pin system, DPS) [43] are employed to monitor the velocity profiles of the baseplate-sample and sample-window interfaces, respectively. More details of the experimental design and diagnostic techniques [44] are described in the Supplemental Material (SM) [45].

Representative experimental records for MCOP-II and DPS-II are shown in the upper and lower panels of Fig. 1, respectively. Both exhibit distinct step-rise signals, which

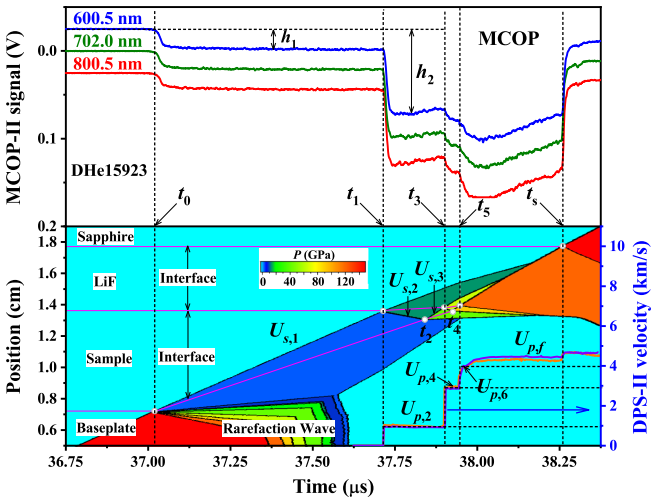

FIG. 1. Upper panel: time-resolved self-emission of the shocked sample recorded by MCOP-II at wavelengths of 600.5, 702.0, and 800.5 nm. Lower panel: velocity histories of sample-window interface recorded by DPS-II (the purple and orange solid step-rise signals), together with the position-time diagram from 1D hydrodynamic simulations. The 1D simulations indicate a clearly physical picture for the shock-wave reverberations and positions of interfaces. $U_{s,i}(i = 1, 2, 3, \ldots)$ represent the slope of the trajectory of the shock wave, namely the shock velocity of the ith shock. The color contour represents shock pressures. The experimental measurements provide the shock timing $(t_0, t_1, t_3, t_5, \ldots)$ and the actual particle velocities of the even-numbered shocked sample $(U_{p,2}, U_{p,4}, U_{p,6}, \ldots)$ with the LiF refractive index correction [46].

provides a clear picture of the shock reverberations. A one-dimensional (1D) fluid dynamics simulation was performed to help in analyzing the experimental signals and the shock-reverberation processes. When the shock wave breaks out into the sample from the baseplate (t_0), the D_2-He sample will be driven to a state on its principal Hugoniot, and this will be accompanied by an abrupt increase in emission intensity, as indicated by the MCOP-II signal. When the first shock arrives at the sample-window interface (t_1), a reflected shock wave $U_{s,2}$ is generated, and this propagates back into the sample. At the same time, a transmitted shock wave enters the window. The sample is reshocked to a state with a higher pressure and temperature, which thereby causes a further rise in the MCOP-II signal. Meanwhile, the sample-window interface is accelerated up to a steady speed, resulting in the first step rise of the DPS-II signal. Based on the continuity condition at the interfaces, this speed is equal to the particle velocity of the second shocked sample $U_{p,2}$. The second shock wave is reflected back when it arrives at the baseplate-sample interface (t_2), which compresses the sample for a third time (the third shock $U_{s,3}$). The above reverberation processes of the shock wave moving between the baseplate-sample and sample-window interfaces repeat until the sample reaches the peak or final state ($U_{p,f}$). The good agreement between the MCOP and DPS signals for the shock reflection timings ensures the accuracy of the experimental measurements. The multishock states, including shock velocities, pressures, and densities, can be directly deduced using the impedance-matching method. The details of the inferences of the multishock states, along with an uncertainty analysis [47,48], are presented in the Part 5 in the SM [45].

The obtained multishock EOS for three shot experiments are given in Table S1 of the SM [45], covering a pressure and temperature range of 2–120 GPa and 3400–7400 K. Thus, the present work significantly expands the scope of the experimental data and improves the experimental constraints on the H_2-He EOS at extreme conditions. First, the present experimental results allow a direct comparison of the compressibilities $\eta = \rho/\rho_0$ of D_2-He mixtures with different helium concentrations, as shown in Fig. S9. The multishock compressibility of the D_2-He mixture with a 50% helium concentration is smaller than that for a 25% helium concentration. Figure 2 and Fig. S7 show a comparison of the experimental P–ρ data with the theoretical multishock curves calculated by various EOS models, including the SCVH [7] and SESAME [49] chemical models and the REOS.3 [9] and CMS [10] multiphase EOSs. These models show small differences at low densities of $\rho < 0.2$ g/cm^3 compared to the experimental data. This is also supported by the independent experimental temperature measurements, as shown in Fig. S11 (the deduction of shock temperatures from MCOP signals can be found in the SM [45]). Note that

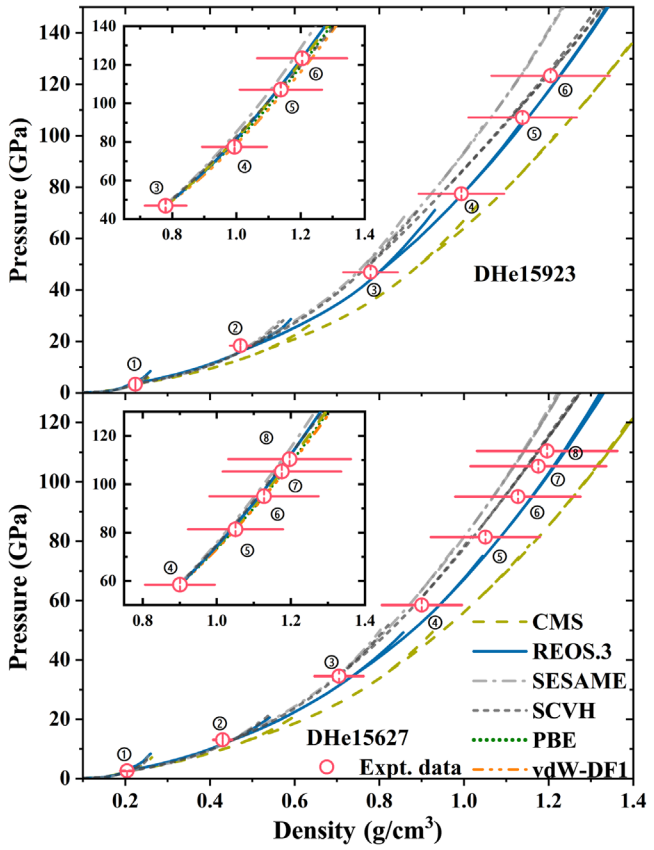

FIG. 2. The experimental multishock EOSs of the D_2-He mixture (D_2:He = 1:1) for shots DHe15923 and DHe15627 are compared to theoretical multishock curves and theoretical isentropes (the insets). The numbers in circles indicate the ith shock state. The theoretical isentropes of shots DHe15923 and DHe15627 start from the third and fourth shock states, respectively.

the EOS data from REOS.3 and CMS in this domain are mainly generated by chemical models. Thus, the chemical models can be used as useful alternatives for generating the EOS at low densities (specifically, below 0.1 g/cm^3), within which the computing resources for *ab initio* simulations increase dramatically.

With the increase of density, obvious differences among these models appear. The SESAME model shows a stiffer behavior (lower compressibility) among these models. The SCVH model is softer than the SESAME model. The difference between these two chemical models may arise from the differences in the potentials used or the construction of the free-energy functions. The CMS model is softer compared to the REOS.3 model. Both EOSs are based on the combination of first-principles molecular dynamics (FPMD) calculations and the semianalytical EOS models. Nevertheless, there exists a large gap between FPMD and chemical-model data in CMS (0.05–0.3 g/cm^3 for H and 0.1–1.0 g/cm^3 for He), meaning that the interpolated connection between them may induce the deviations from REOS.3. Present experiments provide an important dataset for evaluating these models. It is found that these EOS models and the experimental results show reasonable agreement within the errors, implying that the models follow the right trend in this regime.

The quasi-isentropic EOS data is another important experimental constraint, and this has direct astrophysical applications because the interiors of giant planets are entirely convective, and their internal temperatures therefore follow an isentrope. The multiple reverberation compression provides a unique compression path from shock-adiabatic to quasi-isentropic compressions. To illustrate more directly, we calculate the changes in entropy during multiple reverberation compressions with the aid of the CMS model (Fig. S12 of the SM [45]). The entropy increases obviously during the first and second compressions, whereas the entropy hardly changes after the third or fourth compressions.

The insets of Fig. 2 show a comparison between our experimental data and the theoretical isentropes in the range of 50–120 GPa. The isentropes are calculated according to the first-order differential equation [63]

$$\left(\frac{\partial T}{\partial \rho}\right)_s = \frac{T}{\rho^2}\frac{(\frac{\partial P}{\partial T})_\rho}{(\frac{\partial E}{\partial T})_\rho}. \tag{1}$$

The initial temperature and density of the isentropes start from the third or fourth compression state. It is evident that the experimental data are in fairly good agreement with the theoretical isentropes, demonstrating once again the quasi-isentropic nature of the multiple reverberation compressions. Note that the CMS and REOS.3 calculations also show excellent agreement. The reason for this is that the EOS data from CMS and REOS.3 in this region are entirely generated by FPMD simulations with the same Perdew-Burke-Ernzerhof (PBE) functional [50]. Moreover, the present FPMD calculations [51–53,59–61] with PBE and van der Waals (vdW-DF1) [62] functionals for a real D_2-He mixture (computational details can be found in the SM [45]) basically coincide with the REOS.3 results, so the nonlinear mixing effect and vdW interactions may not play dominant roles within this regime.

The quasi-isentropic nature of multiple reverberation compressions offers an opportunity to obtain the sound velocity. According to the definition of the sound velocity,

$$C_S = \sqrt{-V^2\left(\frac{\partial P}{\partial V}\right)_S}, \tag{2}$$

where the subscript S represents entropy, it is closely related to the isentropic EOS. Because of the limited number of experimental EOS data points, we adopt a fitting procedure to deal with the partial derivative. Therefore, we need first to construct an analytical isentropic equation that can reproduce the experimental data

well. In the following, we will demonstrate a power-form isentropic equation,

$$P = A\rho^k, \tag{3}$$

where A is a constant and k is the isentropic exponent. Generally, the isentropic exponent is defined as

$$k = (\partial \ln P/\partial \ln \rho)_S. \tag{4}$$

If k is constant, the system is described by the isentropic equation [Eq. (3)]. To verify this, we calculate k along the theoretical isentropes in Fig. 2 by using Eq. (4), as shown in Fig. S13. Obviously, the value of k is almost constant, especially for REOS.3 and vdW-DF1 (varying by less than 3%). Through a nonlinear least-squares fitting to the quasi-isentropic data with Eq. (3), the parameters A and k are determined. Fig. S14 shows that the power-form isentropic equation can reproduce the experimental data well, which further proves the rationality of treating k as a constant. Within the quasi-isentropic regime, D_2 has almost fully dissociated as illustrated by the pair-correlation functions from FPMD (Fig. S15), while the ionization of helium can be neglected [54] and the ionization of deuterium is noticeable based on the average atom model [55] and FPMD calculations [56–58] (see section 13 of the SM [45]). As shown in Fig. S18, the variation of dissociation and ionization in this regime is weak and may be responsible for the small change of k. Note that Eq. (3) is formally identical to the isentropic equation of an ideal gas. However, the dense D_2-He mixture is definitely nonideal, and the resulting value of k (around 2.26) is larger than the ideal-gas isentropic exponent $k = C_p/C_v$ (5/3 for the monoatomic system).

The experimental sound velocity can be directly determined through the experimentally constrained isentropic equation. In Fig. 3 and Fig. S8, we compare the present sound velocities to the theoretical calculations (the computational details for the sound velocity are provided in the SM [45]). The insets show the comparisons in the $C_s - \rho$ space. The differences in sound velocities between the various models in the range of 50–120 GPa are more obvious than those of the isentropes shown in Fig. 2, as the sound velocity is the derivation of the EOS. This makes the sound velocity more important for validating theoretical models. The comparison results show that the theoretical calculations are within the experimental errors in the probed pressure range. Moreover, the sound velocities at high pressures up to 1 TPa are calculated by theoretical models. The differences between the models gradually enlarge when approaching TPa pressures. Future experiments to measure the sound velocities in the TPa pressure range are highly desirable for further discriminating the EOS models.

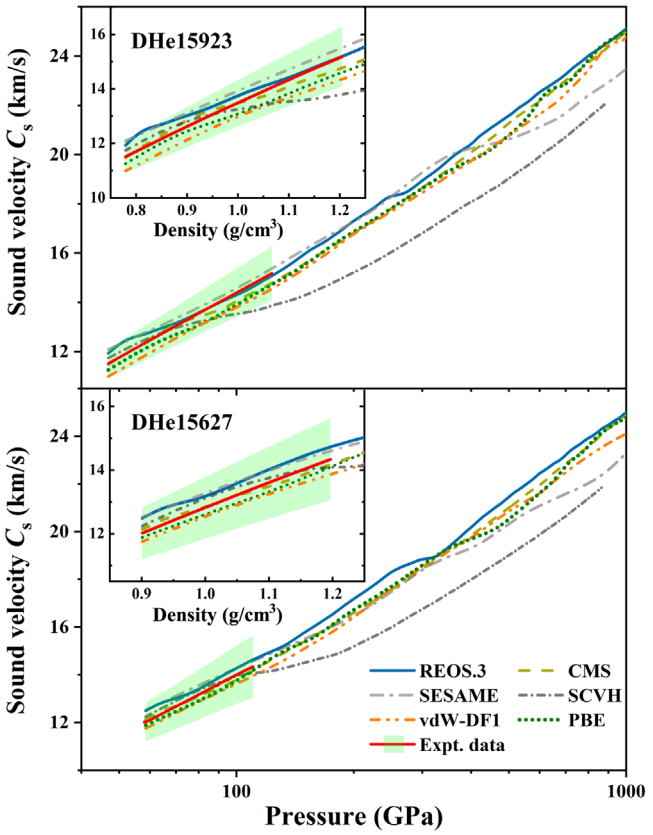

FIG. 3. The experimental sound velocities versus pressure and density (the insets) of D_2-He mixture (D_2:He = 1:1) for shots DHe15923 and DHe15627 are compared to the theoretical calculations. The theoretical sound velocities are calculated along the isentropes in Fig. 2. The shaded area represents a 1σ confidence interval.

The high-pressure sound velocities of hydrogen and helium are of significance for understanding the seismic structure of giant planets. The currently available sound velocity data for H_2, D_2, and He are summarized in Fig. 4, together with the present D_2-He mixture results. The previous data from Brillouin scattering measurements in diamond anvil cell (DAC) experiments [38,39] and the shock-overtake technique in gas-gun experiments [41] are within 30 GPa and 5.5 kK, which is mainly relevant to the molecular-atomic envelope (region I) of the interior of Jupiter. The present experiments extensively expand the ranges of sound velocities up to 120 GPa and beyond 10 kK, reaching a transition zone (region II) that encompasses the pressure ionization of hydrogen. These data are comparable to the recent experimental data obtained based on the unsteady-wave technique using a high-power laser [40]. Nevertheless, the sound velocities obtained using laser-driven shocks are along the principal Hugoniot states of liquid deuterium and are accompanied by rapid temperature rises, as explicitly indicated by the right panel of Fig. 4. Consequently, the experimental conditions of laser shock are far away from the Jupiter adiabat. Conversely,

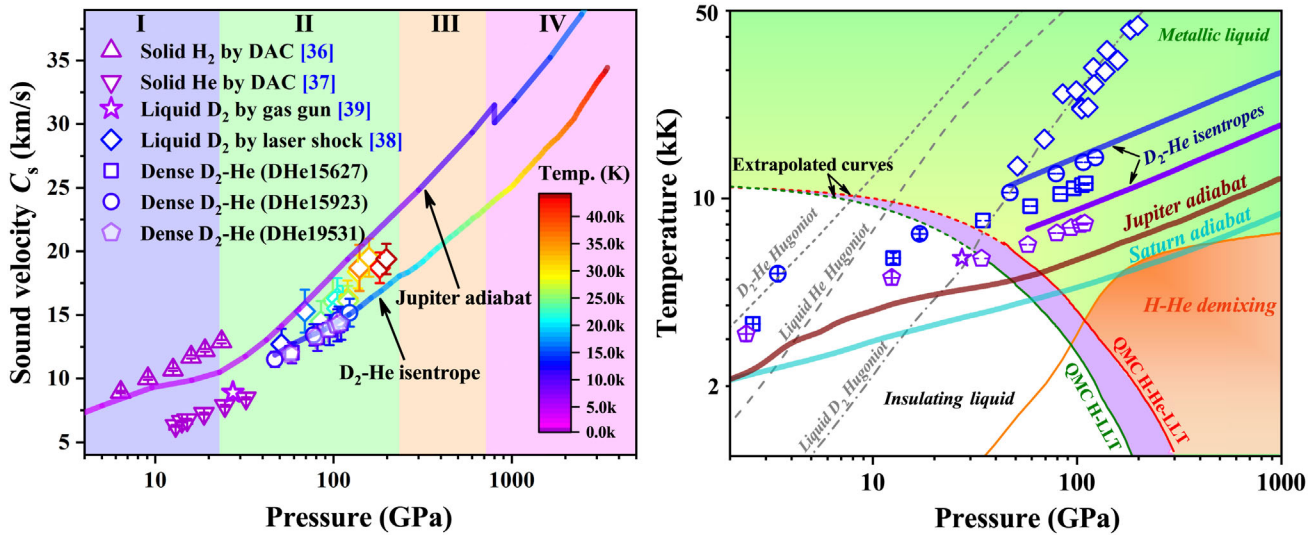

FIG. 4. Left panel: present sound velocities of the D_2-He mixture are compared to the available experimental data of pure H_2, D_2, and He; the symbol color indicates the temperatures calculated by REOS.3. The Jupiter adiabat calculated by French *et al.* [64] and the D_2-He mixture isentrope by REOS.3 calculations are also shown. Regions I, II, III, and IV correspond to the molecular-atomic envelope, the transition zone encompassing the pressure ionization of hydrogen, the metallic hydrogen envelope, and the diluted Z-rich core in the interior of Jupiter, based on the four-layer Jupiter interior model of Debras *et al.* [12]; Right panel: phase diagram for hydrogen and hydrogen-helium mixtures, together with the liquid-liquid transition (LLT) [65] and H-He demixing [66] boundaries. Also shown are the experimental EOS of D_2-He mixtures (the temperatures beyond the second shock were estimated from REOS.3) and liquid D_2, theoretical Hugoniots of liquid D_2, liquid He, and D_2-He mixture calculated by REOS.3, and the Jupiter and Saturn adiabats [67,68].

our study demonstrates the ability to obtain isentropic sound velocities, and the phase diagram illustrates the experimental conditions are more relevant to giant planets interiors. Additionally, the shock temperatures of the D_2-He mixture with a 75% deuterium concentration are smaller than those for a 50% deuterium concentration, thus much closer to Jupiter's and Saturn's interior conditions. Such information will provide a firmer basis for establishing the structure and dynamic properties of gas giant planets and their evolution.

In summary, we carried out multiple reverberation compression experiments on dense gaseous D_2-He mixtures, expanding the experimental multishock pressures up to 120 GPa and reshock temperatures to 7400 K, which is directly relevant to planetary interiors. The multiple reverberation compression produces a unique compression path from shock adiabatic to quasi-isentropic compressions, which enables the measurements of the sound velocities from 50 to 120 GPa. The experimental dataset demonstrates the rationality of the primary models for astrophysics in the probed pressure regime. Furthermore, the predictions from different models vary dramatically when approaching TPa pressures, which calls for future experiments to expand the EOS and sound velocities to TPa pressures and thus provide more stringent constraints for the theoretical models of the Jovian metallic hydrogen envelope.

We thank our colleagues for the gas-gun operation, experimental diagnosis, and devices. We are grateful to anonymous reviewers for their constructive suggestions. We especially appreciate Professor Mu Li and Dr. Cheng-Jin Huang for fruitful discussions. This work was supported by the National Natural Science Foundation of China (Grant Nos. 11674292, 11672274, 11802280, 11872057, and 11804284) and the Science Challenge Project (Grant No. TZ2016001). The calculations were carried out on TianHe-2 at the LvLiang Cloud Computing Center in China.

*Corresponding author.
zhiguo_li@foxmail.com
†Corresponding author.
chenqf01@gmail.com
‡Corresponding author.
lei_liuchn@163.com

[1] J. M. McMahon, M. A. Morales, C. Pierleoni, and D. M. Ceperley, Rev. Mod. Phys. **84**, 1607 (2012).
[2] J. J. Fortney and N. Nettelmann, Space Sci. Rev. **152**, 423 (2010).
[3] D. Saumon and T. Guillot, Astrophys. J. **609**, 1170 (2004).
[4] Q. Ma, J. Dai, D. Kang, M. S. Murillo, Y. Hou, Z. Zhao, and J. Yuan, Phys. Rev. Lett. **122**, 015001 (2019).
[5] B. Lu, D. Kang, D. Wang, T. Gao, and J. Dai, Chin. Phys. Lett. **36**, 103102 (2019).
[6] L. Liu, Q.-F. Chen, Y.-J. Gu, W. Zhang, Z.-G. Li, C.-J. Li, Z.-Q. Wang, G.-J. Li, Y.-S. Lan, and X.-R. Chen, Appl. Phys. Lett. **115**, 231905 (2019).
[7] D. Saumon, G. Chabrier, and H. M. van Horn, Astrophys. J. Suppl. Ser. **99**, 713 (1995).

[8] B. Militzer and W. B. Hubbard, Astrophys. J. **774**, 148 (2013).

[9] A. Becker, W. Lorenzen, J. J. Fortney, N. Nettelmann, M. Schöttler, and R. Redmer, Astrophys. J. Suppl. Ser. **215**, 21 (2014).

[10] G. Chabrier, S. Mazevet, and F. Soubiran, Astrophys. J. **872**, 51 (2019).

[11] Y. Miguel, T. Guillot, and L. Fayon, Astron. Astrophys. **596**, A114 (2016).

[12] F. Debras and G. Chabrier, Astrophys. J. **872**, 100 (2019).

[13] W. J. Nellis, N. C. Holmes, A. C. Mitchell, R. J. Trainor, G. K. Governo, M. Ross, and D. A. Young, Phys. Rev. Lett. **53**, 1248 (1984).

[14] C. T. Seagle, W. D. Reinhart, A. J. Lopez, R. J. Hickman, and T. F. Thornhill, J. Appl. Phys. **120**, 125902 (2016).

[15] S. T. Weir, A. C. Mitchell, and W. J. Nellis, Phys. Rev. Lett. **76**, 1860 (1996).

[16] J. Zheng, Q. F. Chen, Y. J. Gu, J. T. Li, Z. G. Li, C. J. Li, and Z. Y. Chen, Phys. Rev. B **95**, 224104 (2017).

[17] J. Tang, Y. J. Gu, Q. F. Chen, Z. G. Li, J. Zheng, C. J. Li, and J. T. Li, Phys. Rev. B **97**, 140101(R) (2018).

[18] G. V. Boriskov, A. I. Bykov, R. I. Il'kaev, V. D. Selemir, G. V. Simakov, R. F. Trunin, V. D. Urlin, A. N. Shuikin, and W. J. Nellis, Phys. Rev. B **71**, 092104 (2005).

[19] V. E. Fortov, R. I. Ilkaev, V. A. Arinin, V. V. Burtzev, V. A. Golubev, I. L. Iosilevskiy, V. V. Khrustalev, A. L. Mikhailov, M. A. Mochalov, V. Y. Ternovoi, and M. V. Zhernokletov, Phys. Rev. Lett. **99**, 185001 (2007).

[20] M. A. Mochalov, R. I. Il'kaev, V. E. Fortov, A. L. Mikhailov, V. A. Arinin, A. O. Blikov, V. A. Komrakov, I. P. Maksimkin, V. A. Ogorodnikov, and A. V. Ryzhkov, JETP Lett. **107**, 168 (2018).

[21] M. A. Mochalov, R. I. Il'kaev, V. E. Fortov, A. L. Mikhailov, V. A. Arinin, A. O. Blikov, V. A. Ogorodnikov, A. V. Ryzhkov, V. A. Komrakov, and I. P. Maksimkin, JETP Lett. **108**, 656 (2018).

[22] M. D. Knudson and M. P. Desjarlais, Phys. Rev. Lett. **118**, 035501 (2017).

[23] M. D. Knudson, D. L. Hanson, J. E. Bailey, C. A. Hall, J. R. Asay, and W. W. Anderson, Phys. Rev. Lett. **87**, 225501 (2001).

[24] M. D. Knudson, D. L. Hanson, J. E. Bailey, C. A. Hall, J. R. Asay, and C. Deeney, Phys. Rev. B **69**, 144209 (2004).

[25] D. G. Hicks, T. R. Boehly, P. M. Celliers, J. H. Eggert, S. J. Moon, D. D. Meyerhofer, and G. W. Collins, Phys. Rev. B **79**, 014112 (2009).

[26] A. Fernandez-Pañella, M. Millot, D. E. Fratanduono, M. P. Desjarlais, S. Hamel, M. C. Marshall, D. J. Erskine, P. A. Sterne, S. Haan, T. R. Boehly, G. W. Collins, J. H. Eggert, and P. M. Celliers, Phys. Rev. Lett. **122**, 255702 (2019).

[27] S. Brygoo, M. Millot, P. Loubeyre, A. E. Lazicki, S. Hamel, T. Qi, P. M. Celliers, F. Coppari, J. H. Eggert, D. E. Fratanduono, D. G. Hicks, J. R. Rygg, R. F. Smith, D. C. Swift, G. W. Collins, and R. Jeanloz, J. Appl. Phys. **118**, 195901 (2015).

[28] T. Sano *et al.*, Phys. Rev. B **83**, 054117 (2011).

[29] P. Loubeyre, S. Brygoo, J. Eggert, P. M. Celliers, D. K. Spaulding, J. R. Rygg, T. R. Boehly, G. W. Collins, and R. Jeanloz, Phys. Rev. B **86**, 144115 (2012).

[30] J. Eggert, S. Brygoo, P. Loubeyre, R. S. McWilliams, P. M. Celliers, D. G. Hicks, T. R. Boehly, R. Jeanloz, and G. W. Collins, Phys. Rev. Lett. **100**, 124503 (2008).

[31] P. Davis, T. Doppner, J. R. Rygg, C. Fortmann, L. Divol, A. Pak, L. Fletcher, A. Becker, B. Holst, P. Sperling, R. Redmer, M. P. Desjarlais, P. Celliers, G. W. Collins, O. L. Landen, R. W. Falcone, and S. H. Glenzer, Nat. Commun. **7**, 11189 (2016).

[32] J. Vorberger, I. Tamblyn, B. Militzer, and S. A. Bonev, Phys. Rev. B **75**, 024206 (2007).

[33] Z.-G. Li, W. Zhang, Z.-J. Fu, J.-Y. Dai, Q.-F. Chen, and X.-R. Chen, Phys. Plasmas **24**, 052903 (2017).

[34] Z.-G. Li, Q.-F. Chen, Y.-J. Gu, J. Zheng, and X.-R. Chen, AIP Adv. **6**, 105309 (2016).

[35] Z.-G. Li, Q.-F. Chen, Y.-J. Gu, J. Zheng, W. Zhang, L. Liu, G.-J. Li, Z.-Q. Wang, and J.-Y. Dai, Phys. Rev. B **98**, 064101 (2018).

[36] Y. J. Gu, Q. F. Chen, L. C. Cai, Z. Y. Chen, J. Zheng, and F. Q. Jing, J. Chem. Phys. **130**, 184506 (2009).

[37] T. S. Duffy, W. L. Vos, C. S. Zha, R. J. Hemley, and H. K. Mao, Science **263**, 1590 (1994).

[38] C.-S. Zha, T. S. Duffy, H.-K. Mao, and R. J. Hemley, Phys. Rev. B **48**, 9246 (1993).

[39] C.-S. Zha, H.-K. Mao, and R. J. Hemley, Phys. Rev. B **70**, 174107 (2004).

[40] D. E. Fratanduono, M. Millot, A. F. Pañella, P. A. Sterne, G. W. Collins, D. G. Hicks, J. H. Eggert, T. R. Boehly, and P. M. Celliers, Phys. Plasmas **26**, 012710 (2019).

[41] N. C. Holmes, W. J. Nellis, and M. Ross, AIP Conf. Proc. **429**, 61 (1998).

[42] N. C. Holmes, Rev. Sci. Instrum. **66**, 2615 (1995).

[43] J. Weng, H. Tan, X. Wang, Y. Ma, S. Hu, and X. Wang, Appl. Phys. Lett. **89**, 111101 (2006).

[44] J. Weng, T. Tao, S. Liu, H. Ma, X. Wang, C. Liu, and H. Tan, Rev. Sci. Instrum. **84**, 113103 (2013).

[45] See Supplemental Material, which includes Refs. [6,7,9,10,16,17,31,32,42–44,46–62], at http://link.aps.org/supplemental/10.1103/PhysRevLett.126.075701 for more experimental information and a detailed description of the FPMD calculations.

[46] B. J. Jensen, D. B. Holtkamp, P. A. Rigg, and D. H. Dolan, J. Appl. Phys. **101**, 013523 (2007).

[47] M. D. Knudson, M. P. Desjarlais, R. W. Lemke, T. R. Mattsson, M. French, N. Nettelmann, and R. Redmer, Phys. Rev. Lett. **108**, 091102 (2012).

[48] T. S. Duffy and T. J. Ahrens, J. Appl. Phys. **82**, 4259 (1997).

[49] G. I. Kerley, Phys. Earth Planet. Inter. **6**, 78 (1972).

[50] J. P. Perdew, K. Burke, and M. Ernzerhof, Phys. Rev. Lett. **77**, 3865 (1996).

[51] G. Kresse and J. Furthmüller, Phys. Rev. B **54**, 11169 (1996).

[52] P. E. Blöchl, Phys. Rev. B **50**, 17953 (1994).

[53] G. Kresse and D. Joubert, Phys. Rev. B **59**, 1758 (1999).

[54] P. M. Celliers, P. Loubeyre, J. H. Eggert, S. Brygoo, R. S. McWilliams, D. G. Hicks, T. R. Boehly, R. Jeanloz, and G. W. Collins, Phys. Rev. Lett. **104**, 184503 (2010).
[55] Y. Hou, F. Jin, and J. Yuan, Phys. Plasmas **13**, 093301 (2006).
[56] R. Kubo, J. Phys. Soc. Jpn. **12**, 570 (1957).
[57] D. A. Greenwood, Proc. Phys. Soc. **71**, 585 (1958).
[58] N. V. Smith, Phys. Rev. B **64**, 155106 (2001).
[59] A. Baldereschi, Phys. Rev. B **7**, 5212 (1973).
[60] S. Nosé, J. Chem. Phys. **81**, 511 (1984).
[61] W. G. Hoover, Phys. Rev. A **31**, 1695 (1985).
[62] M. Dion, H. Rydberg, E. Schröder, D. C. Langreth, and B. I. Lundqvist, Phys. Rev. Lett. **92**, 246401 (2004).
[63] A. Becker, N. Nettelmann, B. Holst, and R. Redmer, Phys. Rev. B **88**, 045122 (2013).
[64] M. French, A. Becker, W. Lorenzen, N. Nettelmann, M. Bethkenhagen, J. Wicht, and R. Redmer, Astrophys. J. Suppl. Ser. **202**, 5 (2012).
[65] G. Mazzola, R. Helled, and S. Sorella, Phys. Rev. Lett. **120**, 025701 (2018).
[66] M. Schottler and R. Redmer, Phys. Rev. Lett. **120**, 115703 (2018).
[67] N. Nettelmann, B. Holst, A. Kietzmann, M. French, and R. Redmer, Astrophys. J. **683**, 1217 (2008).
[68] N. Nettelmann, R. Püstow, and R. Redmer, Icarus **225**, 548 (2013).